

RESEARCH ARTICLE

Open Access



Thyroid imaging reporting and data system with MRI morphological features for thyroid nodules: diagnostic performance and unnecessary biopsy rate

Tingting Zheng^{1†}, Yuan Zhang^{1†}, Hao Wang¹, Lang Tang², Xiaoli Xie³, Qingyin Fu², Pu-Yeh Wu⁴ and Bin Song^{1*}

Abstract

Background To assess MRI-based morphological features in improving the American College of Radiology Thyroid Imaging Reporting and Data System (ACR-TIRADS) for categorizing thyroid nodules.

Methods A retrospective analysis was performed on 728 thyroid nodules (453 benign and 275 malignant) that post-operative pathology confirmed. Univariate and multivariate logistic regression analyses were used to find independent predictors of MRI morphological features in benign and malignant thyroid nodules. The improved method involved increasing the ACR-TIRADS level by one when there are independent predictors of MRI-based morphological features, whether individually or in combination, and conversely decreasing it by one. The study compared the performance of conventional ACR-TIRADS and different improved versions.

Results Among the various MRI morphological features analyzed, restricted diffusion and reversed halo sign were determined to be significant independent risk factors for malignant thyroid nodules (OR=45.1, 95% CI=23.2–87.5, $P < 0.001$; OR=38.0, 95% CI=20.4–70.7, $P < 0.001$) and were subsequently included in the final assessment of performance. The areas under the receiver operating characteristic curves (AUCs) for both the conventional and four improved ACR-TIRADSs were 0.887 (95% CI: 0.861–0.909), 0.945 (95% CI: 0.926–0.961), 0.947 (95% CI: 0.928–0.962), 0.945 (95% CI: 0.926–0.961) and 0.951 (95% CI: 0.932–0.965), respectively. The unnecessary biopsy rates for the conventional and four improved ACR-TIRADSs were 62.8%, 30.0%, 27.1%, 26.8% and 29.1%, respectively, while the malignant missed diagnosis rates were 1.1%, 2.8%, 3.7%, 5.4% and 1.2%.

Conclusions MRI morphological features with ACR-TIRADS has improved diagnostic performance and reduce unnecessary biopsy rate while maintaining a low malignant missed diagnosis rate.

Key points

- This study used MRI morphological features to improve College of Radiology Thyroid Imaging Reporting and Data System (ACR-TIRADS).

[†]Tingting Zheng and Yuan Zhang contributed equally to this work and share the first authorship.

*Correspondence:

Bin Song

songbin@fudan.edu.cn

Full list of author information is available at the end of the article



- The performance of the improved ACR-TIRADS is superior to that of the conventional ACR-TIRADS.
- Magnetic resonance morphology features may reduce unnecessary biopsy rate while maintaining a low missed diagnosis rate, thus avoiding unnecessary invasive diagnosis and treatment.

Keywords Magnetic resonance imaging (MRI), Thyroid nodule, Diagnostic performance, Risk stratification, American College of Radiology Thyroid Imaging Reporting and Data System (ACR-TIRADS)

Introduction

Thyroid nodules are a prevalent issue in the endocrine system. The utilization of high-resolution ultrasound has greatly enhanced the ability to detect thyroid nodules and prevalence rates ranging from 19–68% in randomly selected individuals [1–3]. The majority of these nodules are benign, with only a small proportion having clinical significance and approximately 5–10% being confirmed as thyroid cancers [4]. The global prevalence of thyroid cancer continues to increase, currently ranking as the fifth most common form of cancer among American women [5, 6]. The assessment of the benign or malignant nature of thyroid nodules is of utmost importance in selecting the appropriate treatment decision-making, avoiding unnecessary biopsy rate, and improving the disease prognosis [4].

Ultrasonography presently serves as the primary imaging modality for distinguishing between benign and malignant thyroid nodules [7]. Thyroid Imaging Reporting and Data System (TI-RADS) is routinely utilized to effectively manage thyroid nodules by relying on ultrasound risk characteristics [8–10]. Among the various TI-RADSs, the American College of Radiology TI-RADS (ACR-TIRADS) [11] demonstrates superior diagnostic efficacy and a lower unnecessary biopsy rate. Through the examination of a substantial sample size of 37,585 thyroid nodules, Kim et al. [12] found that the ACR-TIRADS had high sensitivity (>90%) for TI-RADS 4 and 5 nodules, with a specificity of only 49%. This low specificity resulted in a considerable number of benign nodules being misdiagnosed, leading to unnecessary biopsy. Therefore, it is imperative to optimize the ACR-TIRADS system to improve specificity and the unnecessary biopsy rate.

Magnetic resonance imaging (MRI) presents numerous advantages, including the ability to conduct imaging in arbitrary planes, the absence of ionizing radiation, exceptional soft tissue contrast, and the capacity to capture various qualitative and quantitative features [13, 14]. Diffusion-weighted imaging (DWI) is a functional imaging technique that provides molecular signatures about pathological conditions and underlying pathophysiological mechanisms by capturing the random Brownian motion of water molecules in tissues [15]. Furthermore, contrast-enhanced (CE) MRI is commonly adopted to

assess the process of lesion enhancement and clearance of contrast material, playing a pivotal role in the identification of both benign and malignant tumors [16–18]. Multiple studies have provided evidence for the effectiveness of multiparametric MRI in diagnosing both benign and malignant thyroid nodules [19–23]. The use of MRI-based features to improve the ACR-TIRADS has not yet been thoroughly investigated in study, though. Therefore, this study aimed to improve the ACR-TIRADS by integrating the MRI-based morphological features, and investigate the efficacy of various improved methods in enhancing the diagnostic accuracy for distinguishing between benign and malignant thyroid nodules, as well as reducing the unnecessary biopsy rate.

Materials and methods

Patients and study design

The ethical committee of Minhang hospital, Fudan University approved this retrospective observational study that informed consent was abandoned, which was carried out in accordance with the guidelines specified in the Declaration of Helsinki.

Retrospective research was done on 931 thyroid nodules from 688 individuals who underwent surgical excision at our facility between January 2017 and December 2022. Inclusion criteria were as follows: (1) patients who underwent preoperative thyroid MRI; (2) patients with postoperative pathological confirmation as benign or malignant. Exclusion criteria were as follows: (1) presence of diffuse bilateral lesions with different pathological types; (2) poor image quality with severe artifacts; (3) patients who underwent FNA or partial thyroidectomy prior to MRI; (4) cases with unclear postoperative pathological findings; (5) incomplete imaging; (6) lesions smaller than 5 mm; (7) absence of preoperative thyroid US or insufficient US images for diagnosis. The surgical indications for thyroid nodules include those categorized as TI-RADS grade ≥ 4 , indicating a high suspicion of thyroid cancer, as well as symptomatic benign thyroid tumors resulting from compression, hyper-functioning thyroid adenomas, or concomitant hyperthyroidism.

Ultimately, the study comprised a total of 463 participants with 728 lesions, consisting of 453 benign lesions and 275 malignant lesions (Fig. 1).

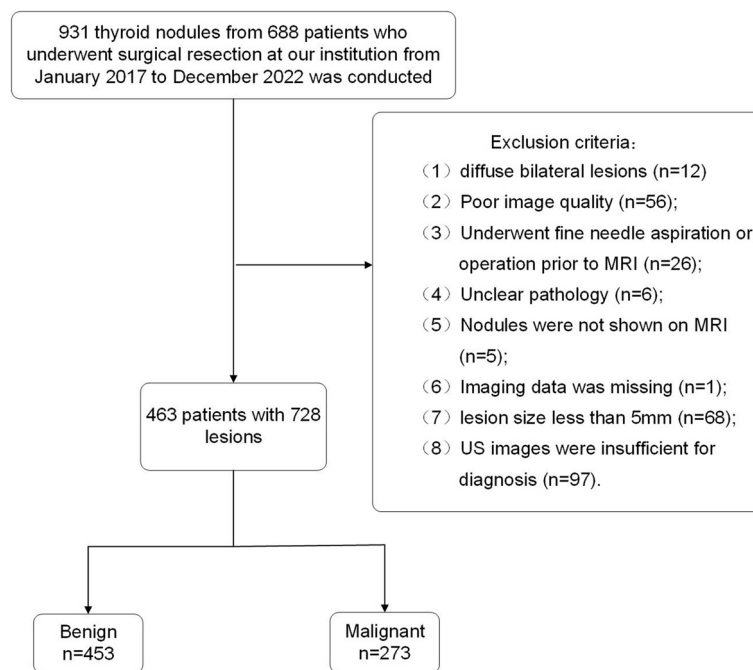


Fig. 1 Flowchart of participant selection

MRI acquisition

MRI examinations were performed on a 1.5 T MRI scanner (Excite HD; GE Healthcare, Milwaukee, WI, USA) equipped with an 8-channel phased-array thyroid coil (Chenguang Medical Technologies, Shanghai, China). The MRI protocols included: (1) coronal fat-suppressed T2-weighted imaging (T2WI) was acquired by a fast recovery fast spin echo (FRFSE) sequence; (2) axial fat-suppressed T2WI; (3) axial T1-weighted imaging (T1WI) was acquired by a FSE sequence; (4) DWI was acquired by a spin-echo echo-planar imaging (SE-EPI) sequence (b -values=0 and 800 s/mm^2); (5) multiphasic CE T1WI was acquired by a fast spoiled gradient echo (FSPGR) sequence at 30 s, 60 s, 120 s, 180 s, 240 s and 300 s after contrast injection. The comprehensive MRI acquisition parameters are shown in Supplementary Table 1. A 15 ml saline flush was administered immediately after the contrast agent (Magen Vixen; Bayer Pharmaceuticals, Berlin, Germany) was injected at a rate of 0.0306 mmol/kg. The total scan time was approximately 14 min.

MRI morphological analysis

Two radiologists (with 6 and 10 years of experience in thyroid MRI), who were unaware of the pathology of lesions, independently evaluated the MRI images using Advantage Workstation 4.5 (GE Healthcare) and Picture Archiving and Communication System (PACS). In case where there was a disagreement between them, a consensus was reached through discussion. The characteristics

of lesion were evaluated as follows: (1) restricted diffusion was defined as lesion with high signal on DWI and low signal on corresponding apparent diffusion coefficient (ADC) maps; (2) reversed halo sign was defined as lesion in the delayed phase of CE-T1WI exhibiting high signal intensity in the peripheral area compared to the central area and a blurred outline.

ACR-TIRADS

Two experienced ultrasonography experts, each with over a decade of experience, conducted a retrospective analysis of the ultrasonography characteristics of thyroid nodules. These experts were unaware of the histopathological results during the analysis. Subsequently, they reached a consensus on the various ultrasonography features, encompassing composition, echogenicity, margin, shape, calcification, aspect ratio, extrathyroidal extension, and suspicious cervical lymph node. The ACR-TIRADS was used to categorize each thyroid nodule. Detailed ACR-TIRADS classification are shown in Supplementary Table 2 and 3.

Improved ACR-TIRADS risk stratification systems

The development of four improved ACR-TIRADS risk stratification systems was facilitated by utilizing the presence or absence of the two MRI-based morphological features in the lesion. The four conditions were as follows: (1) solely exhibiting restricted diffusion; (2) solely displaying the reversed halo sign; (3) manifesting both

restricted diffusion and the reversed halo sign; (4) presenting either restricted diffusion or reversed halo sign. Whenever any of the aforementioned four conditions are present in a nodule, the ACR-TIRADS level is upgraded by one level, and conversely, downgraded by one level (the original TI-RADS categorization of grade 2 is not downgraded, and the original TI-RADS categorization of grade 5 is not upgraded).

Comparison of conventional and improved ACR-TIRADSs

The sensitivity, specificity, accuracy, positive predictive value (PPV), and negative predictive value (NPV) of conventional and different improved ACR-TIRADS were separately calculated.

The unnecessary biopsy rate and malignant missed diagnosis rate were compared between conventional and four improved ACR-TIRADSs. The unnecessary biopsy rate refers to the percentage of benign nodules among those recommended for biopsy according to the ACR-TIRADS guidelines. On the other hand, the malignant missed diagnosis rate represents the percentage of malignant nodules determined to be less than grade 4 according to different ACR-TIRADS system.

Statistical analysis

All statistical analyses were performed using SPSS 26.0 (IBM Corp, Armonk, NY, USA) and MedCalc 19.2.1 (MedCalc Software bv, Ostend, Belgium) software packages. Continuous variables were presented as mean \pm standard deviation (SD), while categorical variables were expressed as percentages. T-test and Chi-square test or Fisher's exact test were employed for comparing continuous and categorical variables, respectively. Kappa concordance test was utilized to evaluate concordance between two radiologists. Receiver operating characteristic (ROC) analysis was conducted to assess the diagnostic performance of different systems, and the area under the ROC curve (AUC) was recorded. Delong test was adopted to compare the AUC values. All statistical tests were two-tailed, and p -values along with 95% confidence interval (CI) were reported. P values < 0.05 were considered statistically significant.

Results

Clinicopathological characteristics

The clinical baseline and pathological data of the patients are shown in Table 1. With the exception of gender, all variables exhibited significant differences in the distribution between benign and malignant nodules. A total of 463 patients (mean age, 51.33 ± 13.85 years) with 728 thyroid nodules were included in the study, and were classified as benign ($n = 453$) or malignant ($n = 275$) based on the pathological findings following surgical resection.

Table 1 Basic clinical information of the 463 patients with 728 thyroid nodules

Characteristics	Benign	Malignant	Total	p value
Age, mean \pm SD, years	55.58 \pm 12.12	44.34 \pm 13.70	51.33 \pm 13.85	$< 0.001^*$
Gender				0.291
Male	114(25.2)	79(28.7)	193(26.5)	
Female	339(74.8)	196(71.3)	535(73.5)	
Number				$< 0.001^*$
Unifocal	82(18.1)	142(51.6)	224(30.8)	
Multifocal	371(81.9)	133(48.4)	504(69.2)	
Location				0.016 [*]
Left lobe	217(47.9)	110(40.0)	327(44.9)	
Right lobe	206(45.5)	154(56.0)	360(49.5)	
Isthmus	30(6.6)	11(4.0)	41(5.6)	
Size				$< 0.001^*$
0.5-1 cm	116(25.6)	124(45.1)	240(33.0)	
1-4 cm	264(58.3)	134(48.7)	398(54.7)	
≥ 4 cm	73(16.1)	17(6.2)	90(12.4)	
Hashimoto's thyroiditis				$< 0.001^*$
Absent	391(86.3)	208(75.6)	599(82.3)	
Present	62(13.7)	67(24.4)	129(17.7)	

Data are expressed as the number of nodules, with percentages in parentheses

Abbreviations: SD standard deviation

* $p < 0.05$

MRI-based morphological features

Table 2 displays the statistical analysis results of MRI-based morphological features. The presence of restricted diffusion ($P < 0.001$, OR = 45.1) and the reversed halo sign ($P < 0.001$, OR = 38.0), both indicating a good agreement (Kappa value, 0.914 and 0.818), were identified as independent predictors for malignant thyroid nodules. Representative images of two MRI morphological features with pathology are shown in Fig. 2.

Diagnostic performance of conventional and improved ACR-TIRADSs

The grading results and malignancy rates of thyroid nodules based on the conventional and improved ACR-TIRADS are shown in Table 3. In the conventional ACR-TIRADS, there were a total of 259 thyroid nodules classified as TI-RADS 4, whereas in the four improved ACR-TIRADSs, the numbers of TI-RADS 4 were 59, 58, 74, and 43 for each respective system. Comparison of the upgraded and downgraded nodules in different improved methods is presented in Supplement Material Table 4.

The ROC curves and AUCs of the conventional and four improved ACR-TIRADS are shown in Fig. 3 and Table 5. The AUCs of conventional and four improved

Table 2 Univariate and multivariate analyses results of benign and malignant thyroid nodules

Characteristics	Benign (n = 453)	Malignant (n = 275)	p	Multivariate Analysis		Kappa
				OR (95%CI)	p	
Restricted diffusion			< 0.001*	45.1(23.2–87.5)	< 0.001*	0.914
Absent	426 (94.0)	49 (17.8)				
Present	27(6.0)	226 (82.2)				
Reversed halo sign			< 0.001*	38.0(20.4–70.7)	< 0.001*	0.818
Absent	434 (95.8)	57 (20.7)				
Present	19 (4.2)	218 (79.3)				

Data are expressed as the number of nodules, with percentages in parentheses

Abbreviations: OR odds ratio, CI confidence interval

* $p < 0.05$

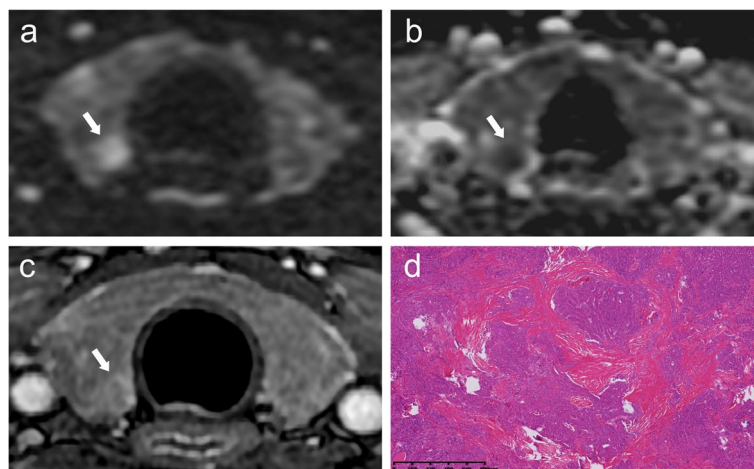


Fig. 2 A 38-year-old female presented with papillary thyroid carcinoma in the right lobe. Axial diffusion-weighted imaging (DWI) (a) and apparent diffusion coefficient (ADC) map (b) demonstrate restricted diffusion of the lesion, indicated by high signal intensity on DWI and low signal intensity on ADC, as denoted by the white arrow. Delayed phase contrast-enhanced T1-weighted imaging (c) reveals central decreased enhancement of the nodule with relative hyperenhancement at the periphery, displaying a reversed halo sign. Histopathological examination using hematoxylin and eosin staining at low magnification (HE, $\times 1$) (d), demonstrates densely distributed tumor cells within a fibrous stromal component

ACR-TIRADS were 0.887 (95% CI: 0.861–0.909), 0.945 (95% CI: 0.926–0.961), 0.947 (95% CI: 0.928–0.962), 0.945 (95% CI: 0.926–0.961) and 0.951 (95% CI: 0.932–0.965) respectively, and between the differences were statistically significant (Delong test, ACR-TIRADS VS improved ACR-TIRADSs, all $p < 0.005$).

The diagnostic performance of the conventional and four improved ACR-TIRADSs is provided in Table 4. Representative ultrasound and MRI images of thyroid nodules are shown in Fig. 4.

Supplementary Table 5 provides the diagnostic performance of the MRI-based morphological features, conventional and four improved ACR-TIRADSs across three different groups based on thyroid nodule size. For nodules of 1 cm or smaller, the accuracy

of ACR-TIRADS was 69.2% (166/240), while the four improved ACR-TIRADSs achieved higher accuracy of 88.4% (212/240), 88.4% (212/240), 88.4% (212/240) and 86.3% (207/240), respectively, surpassing that of the ACR-TIRADS. Among nodules ranging in size from 1 to 4 cm, the accuracy of ACR-TIRADS was 73.4% (292/398), while the four improved ACR-TIRADSs exhibited accuracy of 93.2% (371/398), 93.7% (373/398), 93.7% (373/398), and 93.2% (371/398), respectively. For nodules larger than 4 cm, the accuracy of ACR-TIRADS was 74.4% (67/90), while the four improved ACR-TIRADSs were 90.0% (81/90), 86.7% (78/90), 86.7% (78/90), and 90.0% (81/90), respectively. Supplementary Table 6 provides a detailed overview of the diagnostic performance of the conventional ACR-TIRADS and

Table 3 Classification results of thyroid nodules by the conventional and four improved ACR-TIRADSs

Methods	Classification	Benign	Malignant	Total	Rate of malignancy (%)	<i>p</i> value
ACR-TIRADS	TI-RADS 2	5	0	5	0.0	<0.001*
	TI-RADS 3	253	8	261	3.0	
	TI-RADS 4	172	87	259	33.6	
	TI-RADS 5	23	180	203	88.7	
Restricted diffusion (A)	TI-RADS 2	253	3	256	1.2	<0.001*
	TI-RADS 3	152	18	170	10.6	
	TI-RADS 4	26	33	59	55.9	
	TI-RADS 5	22	221	243	90.9	
Reversed halo sign (B)	TI-RADS 2	251	6	257	2.3	<0.001*
	TI-RADS 3	164	21	185	11.4	
	TI-RADS 4	26	32	58	55.2	
	TI-RADS 5	12	216	228	94.7	
A + B	TI-RADS 2	258	7	265	2.6	<0.001*
	TI-RADS 3	169	32	201	15.9	
	TI-RADS 4	23	51	74	68.9	
	TI-RADS 5	3	185	188	98.4	
A or B	TI-RADS 2	246	2	248	0.8	<0.001*
	TI-RADS 3	147	7	154	4.5	
	TI-RADS 4	29	14	43	32.6	
	TI-RADS 5	31	252	283	89.0	

Abbreviations: ACR American Radiology, TIRADS Thyroid Imaging Reporting and Data System

* $p < 0.05$

four improved ACR-TIRADSs in various pathological types.

The rate of unnecessary biopsy rate and malignant missed diagnosis

The unnecessary biopsy rate and malignant missed diagnosis for the conventional and four improved ACR-TIRADSs are presented in Table 5. ACR-TIRADS had an unnecessary biopsy rate of 62.8% (201/320) and a malignant diagnosis missed rate of 1.1% (8/728). The first three methods significantly reduced the rate of unnecessary biopsies (from 62.8% to 30.0%, 27.1% and 26.8%), but the corresponding missed diagnosis rates were high (from 1.1% to 2.8%, 3.7% and 5.4%, $P < 0.001$). The fourth improved ACR-TIRADS (A or B) had unnecessary biopsy rate of 29.1% and missed diagnosis rate of 1.2% (9/728). The malignant cases missed by the fourth improved ACR-TIRADS are shown in Supplementary Table 7. Among the total of 9 missed cases, 7 were follicular thyroid carcinoma (FTC) and 2 were papillary thyroid carcinoma

(PTC). None of these cases exhibited restricted diffusion or reversed halo sign.

Discussion

In this study, MRI-based morphological features enhanced the diagnostic performance of ACR-TIRADS and considerably decreased the number of nodules categorized as TI-RADS 4 (from 259 to 59, 58, 74, and 43). Among the improved ACR-TIRADSs, the fourth method (A or B) showed the best performance with an AUC of 0.951 compared to 0.887 for conventional ACR-TIRADS ($P < 0.001$). Furthermore, this approach reduced unnecessary biopsy rate to 29.1% without compromising the low malignant missed diagnosis rate (1.2%).

The TI-RADS for thyroid nodules is routinely used for risk stratification and FNA screening of thyroid nodules based on ultrasound characteristics, such as the ACR-TIRADS [11]. A meta-analysis conducted by Castellana M et al. compared the diagnostic performance of different TI-RADS grading system and found that ACR TI-RADS had better performance in selecting thyroid

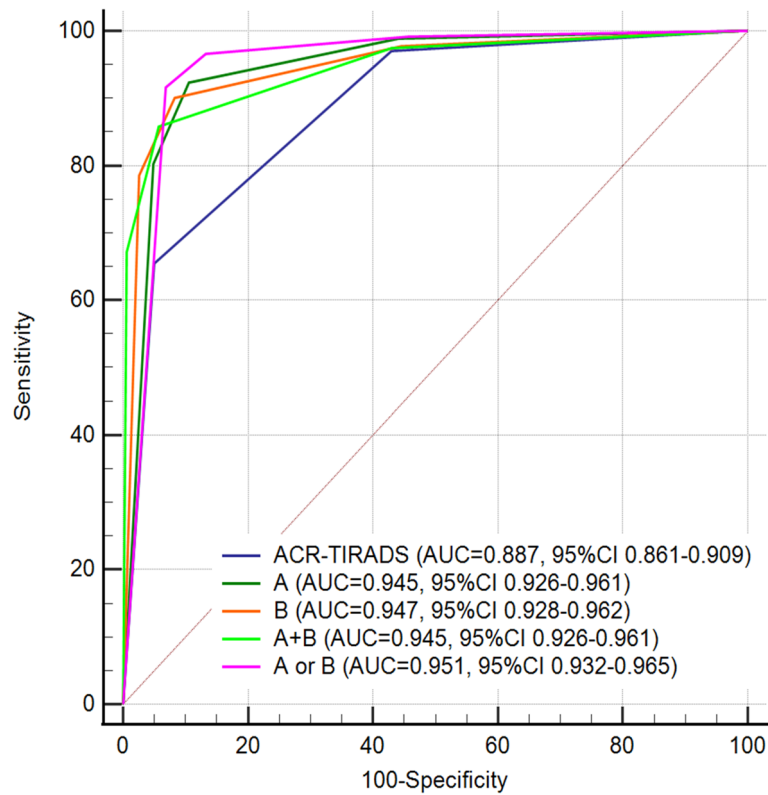


Fig. 3 Receiver operator characteristic curves for conventional and different improved ACR-TIRADS. **A** Restricted diffusion; **B** Reversed halo sign

Table 4 The diagnostic performance of the conventional and four improved ACR-TIRADSs

Methods (cutoff)	Sensitivity	Specificity	Accuracy	PPV	NPV
ACR-TIRADS (≥ 4)	97.1	57.0	72.1	57.8	97.0
Restricted diffusion (A) (≥ 4)	92.4	89.4	90.5	84.1	95.1
Reversed halo sign (B) (≥ 4)	90.2	91.6	91.1	86.7	93.9
A + B (≥ 4)	85.8	94.3	91.1	90.1	91.6
A or B (≥ 4)	96.7	86.8	90.5	81.6	97.8
ACR-TIRADS (≥ 5)	64.6	94.7	83.8	88.2	81.4
Restricted diffusion (A) (≥ 5)	80.4	95.1	87.2	90.9	88.9
Reversed halo sign (B) (≥ 5)	78.5	97.4	90.3	94.7	88.2
A + B (≥ 5)	67.3	99.3	87.2	98.4	83.3
A or B (≥ 5)	92.6	91.6	93.1	94.0	94.8

Data are expressed as percentages

Abbreviations: PPV positive predictive value, NPV negative predictive value, ACR American College of Radiology, TIRADS Thyroid Imaging Reporting and Data System

nodules for FNA [24]. Similar findings were reported in other studies [25–28]. However, ACR-TIRADS has a low specificity of 49% at the optimal cutoff of TR4 and

requires improvement [12]. In recent years, ultrasound has been utilized to improve the diagnostic accuracy of ACR-TIRADS. The study conducted by Huang et al. [29] revealed a strong correlation between thyroid nodules exhibiting lobulated or irregular borders, punctate echogenic foci, and hypoenhancement on contrast-enhanced ultrasound with malignant tumors. The modified TIRADS (AUC=0.863) was considerably superior to ACR-TIRADS (AUC=0.738) in distinguishing between benign and malignant nodules. Luo et al. [30] employed ultrasound radiomics scoring (Rad-score) in conjunction with ACR-TIRADS to assess its efficacy. While Rad-score demonstrated lesser discriminatory ability than ACR-TIRADS in distinguishing between benign and malignant tumors, the combined approach exhibited superior performance compared to either individual method (AUC: 0.913 vs. 0.899). Notably, no studies investigating the utilization of MRI to improve ACR-TIRADS have been identified.

We have made modifications to the ACR-TIRADS system by integrating restricted diffusion and reversed halo sign on MRI. DWI is a non-invasive imaging modality that captures the microscopic and stochastic motion of water molecules within living tissues, enabling the assessment of diffusion characteristics in vivo. It has

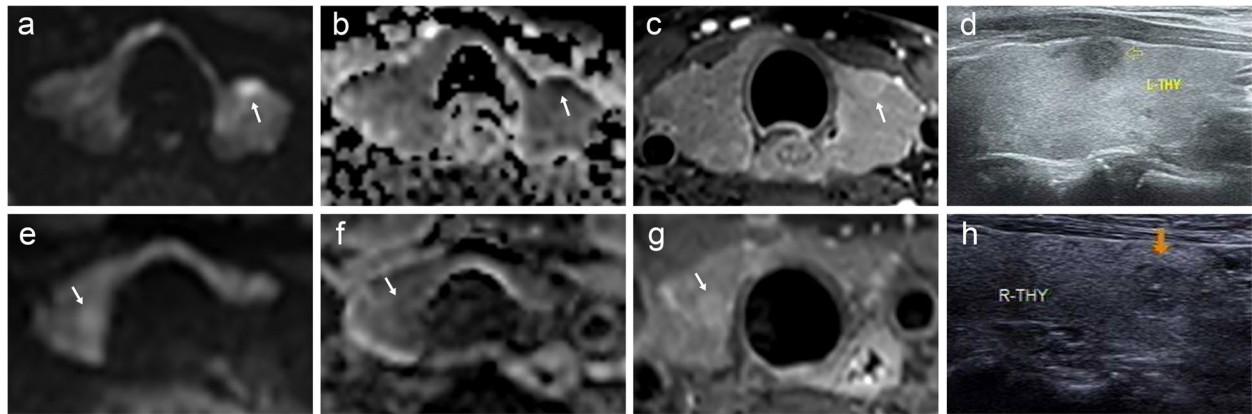


Fig. 4 A 51-year-old female with papillary thyroid carcinoma in the left lobe (**a, b, c** and **d**). Axial diffusion-weighted imaging (DWI) (**a**) and apparent diffusion coefficient (ADC) map (**b**) show restricted diffusion of the lesion (white arrow). The delayed phase contrast-enhanced T1-weighted imaging (**c**) shows reversed halo sign (white arrow). The ultrasound image (**d**) displays a lesion initially classified as ACR-TIRADS grade TI-RADS 4, which has been upgraded to the improved ACR-TIRADS grade of TI-RADS 5, indicating the recommendation for fine needle aspiration biopsy. A 67-year-old female with adenomatous goiter in the right lobe (**e, f, g** and **h**). Axial DWI (**e**) and ADC (**f**) show absence of restricted diffusion (white arrow). The delayed phase contrast-enhanced T1-weighted imaging (**g**) shows a relatively homogeneous enhancement pattern (white arrow). The ultrasound image (**h**) of the lesion, initially classified as ACR-TIRADS grade TI-RADS 4 but subsequently revised to an improved ACR-TIRADS grade TI-RADS 3, obviating biopsy

Table 5 The AUC, unnecessary biopsy rate and malignant missed diagnosis for the conventional and four improved ACR-TIRADSs

Methods	Size (mm)	Benign (n)	Malignant (n)	Total (n)	AUC	P	Unnecessary biopsy rate (%)	Malignant missed diagnosis (%)
ACR-TIRADS		201		320	0.887 (0.861–0.909)	< 0.001*	62.8	1.1 (8/728)
TI-RADS 3	≥ 25	119	4	123			96.7	
TI-RADS 4	≥ 15	72	29	101			71.3	
TI-RADS 5	≥ 10	10	86	96			10.4	
Restricted diffusion (A)		49		169	0.945 (0.926–0.961)	< 0.001*	30.0	2.8 (21/728)
TI-RADS 3	≥ 25	30	5	35			85.7	
TI-RADS 4	≥ 15	9	7	16			56.3	
TI-RADS 5	≥ 10	10	108	118			8.5	
Reversed halo sign (B)		45		166	0.947 (0.928–0.962)	< 0.001*	27.1	3.7 (27/728)
TI-RADS 3	≥ 25	33	12	45			73.3	
TI-RADS 4	≥ 15	7	9	16			43.7	
TI-RADS 5	≥ 10	5	100	105			4.8	
A + B		41		153	0.945 (0.926–0.961)	< 0.001*	26.8	5.4 (39/728)
TI-RADS 3	≥ 25	33	12	45			73.3	
TI-RADS 4	≥ 15	6	12	18			33.3	
TI-RADS 5	≥ 10	2	88	90			2.2	
A or B		53		182	0.951 (0.932–0.965)	< 0.001*	29.1	1.2 (9/728)
TI-RADS 3	≥ 25	30	5	35			19.5	
TI-RADS 4	≥ 15	10	4	14			71.4	
TI-RADS 5	≥ 10	13	120	133			9.7	

Abbreviations: ACR American Radiology, TIRADS Thyroid Imaging Reporting and Data System, P the p value of Delong test between the AUC of conventional and improved ACR-TIRADSs

been recognized as a valuable imaging biomarker for distinguishing benign and malignant tumors [31, 32]. Previous studies have demonstrated that malignant thyroid

nodules exhibited significantly lower ADC values compared to benign nodules, while the optimal threshold for ADC values varies across studies [33–35]. Restricted

diffusion, which refers to the presence of areas with high signal on DWI and low signal on ADC maps. This method provides a straightforward and feasible way for evaluating diffusion restriction without relying on specific ADC thresholds. Pathologically, thyroid cancer is characterized by densely packed tumor cells, which can impede the movement of water molecules and manifest as restricted diffusion. In the delay phase, the reversed halo sign presents as a distinctive imaging features characterized by a contrast enhancement that progresses differently in the central and peripheral areas of the lesion. Specifically, the central region of the lesion demonstrates a more rapid clearance of contrast compared to the peripheral region. In our opinion, this imaging pattern likely suggests that the central active proliferation of neoplastic cells results in washout, while the abundant peripheral tumor stroma causes sustained enhancement.

In our analysis of the diagnostic performance of the four improved ACR-TIRADSs with different cutoff values, we observed that most of the improved ACR-TIRADSs exhibited significantly superior diagnostic efficacy compared to ACR-TIRADS, regardless of the size of nodules. This improvement was particularly notable for nodules ranging from 1 to 4 cm in size.

When assessing the diagnostic performance of the four improved ACR-TIRADSs for different pathological nodule types, we observed that the diagnostic efficacy of ACR-TIRADS for malignant nodules was comparable to that of the four improved ACR-TIRADSs, particularly for PTC, which constituted a significant proportion of cases (98.8% VS 94.8%, 95.6%, 91.3%, and 99.2%). The diagnostic efficacy of both the conventional and improved ACR-TIRADSs was relatively low for FTC. Notably, among the improved ACR-TIRADSs, the fourth method (A or B) exhibited the lowest malignant missed diagnosis rate, but even this method failed to accurately diagnose 7 out of the 9 FTC cases. Therefore, poor efficacy in diagnosing benign and malignant follicular thyroid neoplasms (FTNs) is a limitation of the improved ACR-TIRADSs methods. Distinguishing FTC from follicular thyroid adenoma (FTA) relies primarily on postoperative pathological examination to assess capsule and blood vessel invasion which cannot be diagnosed through ultrasound or FNA [36, 37]. Improvements should be investigated for diagnosis of benign and malignant FTN in the future studies. However, for benign nodules, particularly nodular goiter, the improved ACR-TIRADSs consistently demonstrated a substantial enhancement in diagnostic accuracy (39.9% VS 93.9%, 93.9%, 95.2%, and 91.4%). This improvement significantly reduced the need for additional FNA for benign nodules, thereby minimizing the risks associated with invasiveness and potential bleeding, as indicated in the reduction of unnecessary biopsy rate.

There are several shortcomings in this study. Firstly, our study design is retrospective, which inherently introduces selection bias. Cases were selected after surgical treatment, and the exclusion of many benign nodules and nodules chosen for follow-up after fine needle aspiration biopsy would have influenced the results. Secondly, the MRI-based morphological features utilized in this study are somewhat subjective and may vary based on individual interpretation. Lastly, this study was conducted in a single-center setting, and further research involving multiple centers is necessary to validate the effectiveness of MRI-based morphological features in improving the performance of the ACR-TIRADS risk stratification system.

Conclusion

The study provides evidence that MRI morphological features can help predict malignancy in thyroid nodules and suggests simple methods for combining MRI morphological features with the ACR-TIRADS. The fourth methods improves diagnostic performance reducing the need of biopsy while maintaining a low malignant missed diagnosis rate.

Abbreviations

TI-RADS	Thyroid Imaging Reporting and Data System
ACR	American College of Radiology
MRI	Magnetic resonance imaging
DWI	Diffusion-weighted imaging
CE	Contrast-enhanced
T2WI	T2-weighted imaging
FRFSE	Fast recovery fast spin echo
T1WI	T1-weighted imaging
SE-EPI	Spin-echo echo-planar imaging
FSPGR	Fast spoiled gradient echo
PACS	Picture Archiving and Communication System
ADC	Apparent diffusion coefficient
PPV	Positive predictive value
NPV	Negative predictive value
SD	Standard deviation
ROC	Receiver operating characteristic
AUC	Area under the Receiver operating characteristic curve
CI	Confidence interval
FTC	Follicular thyroid carcinoma
PTC	Papillary thyroid carcinoma

Supplementary Information

The online version contains supplementary material available at <https://doi.org/10.1186/s40644-024-00721-8>.

Supplementary Material 1.

Acknowledgements

We thank the Department of Radiology, Minhang Hospital, Fudan University, for providing the data.

Authors' contributions

All authors and co-authors have significantly contributed. Tingting Zheng: data collection, writing and editing of manuscript. Yuan Zhang: data collection and writing of manuscript. Hao Wang: contribution of data and review of manuscript. Lang Tang: contribution to ultrasound data. Xiaoli Xie: contribution

to pathologic data. Qingyin Fu: contribution to ultrasound data. Pu-Yeh Wu: contribution to review and editing of manuscript. Bin Song: data analysis and writing and review of manuscript.

Funding

This work was supported by the Nature Science Foundation of Shanghai (grant number: 19ZR1446200), Science and Technology Commission of Minhang District, Shanghai (grant number: 2020MHZ034) and Shanghai Municipal Health Commission (grant number: 202140325).

Availability of data and materials

The data sets generated and/or analyzed in the current study were not made public because patients' personal information was included. Available from the corresponding author upon reasonable request.

Declarations

Ethics approval and consent to participate

The institutional review board of Minhang hospital, Fudan University approved this study (approval number: 2021-008-01 K), and informed consent was exempted due to the retrospective nature.

Consent for publication

Not applicable.

Competing interests

The authors declare that they have no competing interests.

Author details

¹Department of Radiology, Minhang Hospital, Fudan University, No 170, Xinsong Road, Minhang District, Shanghai 201199, China. ²Department of Ultrasound, Minhang Hospital, Fudan University, No 170, Xinsong Road, Minhang District, Shanghai 201199, China. ³Department of Pathology, Minhang Hospital, Fudan University, No 170, Xinsong Road, Minhang District, Shanghai 201199, China. ⁴GE Healthcare, MR Research China, Beijing, China.

Received: 16 November 2023 Accepted: 10 June 2024

Published online: 14 June 2024

References

- Guth S, Theune U, Aberle J, Galach A, Bamberger CM. Very high prevalence of thyroid nodules detected by high frequency (13 MHz) ultrasound examination. *Eur J Clin Invest*. 2009;39:699–706.
- Roman BR, Morris LG, Davies L. The thyroid cancer epidemic, 2017 perspective. *Curr Opin Endocrinol Diabetes Obes*. 2017;24:332–6.
- Vaccarella S, Dal Maso L, Laversanne M, Bray F, Plummer M, Franceschi S. The impact of diagnostic changes on the rise in thyroid cancer incidence: a population-based study in selected high-resource countries. *Thyroid*. 2015;25:1127–36.
- Haugen BR, Alexander EK, Bible KC, et al. 2015 American thyroid association management guidelines for adult patients with thyroid nodules and differentiated thyroid cancer: the American thyroid association guidelines task force on thyroid nodules and differentiated thyroid cancer. *Thyroid*. 2016;26:1–133.
- Durante C, Grani G, Lamartina L, Filetti S, Mandel SJ, Cooper DS. The diagnosis and management of thyroid nodules: a review. *JAMA*. 2018;319:914–24.
- Megwalu UC, Moon PK. Thyroid cancer incidence and mortality trends in the United States: 2000–2018. *Thyroid*. 2022;32:560–70.
- Qin P, Wu K, Hu Y, Zeng J, Chai X. Diagnosis of Benign and malignant thyroid nodules using combined conventional ultrasound and ultrasound elasticity imaging. *IEEE J Biomed Health Inform*. 2020;24:1028–36.
- Horvath E, Majlis S, Rossi R, et al. An ultrasonogram reporting system for thyroid nodules stratifying cancer risk for clinical management. *J Clin Endocrinol Metab*. 2009;94:1748–51.
- Kwak JY, Han KH, Yoon JH, et al. Thyroid imaging reporting and data system for US features of nodules: a step in establishing better stratification of cancer risk. *Radiology*. 2011;260:892–9.
- Park JY, Lee HJ, Jang HW, et al. A proposal for a thyroid imaging reporting and data system for ultrasound features of thyroid carcinoma. *Thyroid*. 2009;19:1257–64.
- Tessler FN, Middleton WD, Grant EG, et al. ACR Thyroid Imaging, Reporting and Data System (TI-RADS): white paper of the ACR TI-RADS committee. *J Am Coll Radiol*. 2017;14:587–95.
- Kim DH, Chung SR, Choi SH, Kim KW. Accuracy of thyroid imaging reporting and data system category 4 or 5 for diagnosing malignancy: a systematic review and meta-analysis. *Eur Radiol*. 2020;30:5611–24.
- Turkoglu S, Kayan M. Differentiation between benign and malignant ovarian masses using multiparametric MRI. *Diagn Interv Imaging*. 2020;101:147–55.
- Yun JS, Lee MH, Lee SM, et al. Peripheral nerve sheath tumor: differentiation of malignant from benign tumors with conventional and diffusion-weighted MRI. *Eur Radiol*. 2021;31:1548–57.
- Tan H, Chen J, Zhao YL, et al. Feasibility of intravoxel incoherent motion for differentiating benign and malignant thyroid nodules. *Acad Radiol*. 2019;26:147–53.
- Ramli Hamid MT, Ab Mumin N, Wong YV, Chan WY, Rozalli FI, Rahmat K. The effectiveness of an ultrafast breast MRI protocol in the differentiation of benign and malignant breast lesions. *Clin Radiol*. 2023;78:444–50.
- Li HM, Feng F, Qiang JW, et al. Quantitative dynamic contrast-enhanced MR imaging for differentiating benign, borderline, and malignant ovarian tumors. *Abdom Radiol (NY)*. 2018;43:3132–41.
- Zhou J, Zhang Y, Chang KT, et al. Diagnosis of benign and malignant breast lesions on DCE-MRI by using radiomics and deep learning with consideration of peritumor tissue. *J Magn Reson Imaging*. 2020;51:798–809.
- Monisha V, Rache Gowda N, Anil Kumar S. The role of diffusion-weighted magnetic resonance imaging in differentiating benign from malignant thyroid nodules: a descriptive observational study. *Cureus*. 2022;14:e30493.
- Sharafeldeen A, Elsharkawy M, Khaled R, et al. Texture and shape analysis of diffusion-weighted imaging for thyroid nodules classification using machine learning. *Med Phys*. 2022;49:988–99.
- Shi R, Yao Q, Wu L, et al. T2* mapping at 3.0T MRI for differentiation of papillary thyroid carcinoma from benign thyroid nodules. *J Magn Reson Imaging*. 2016;43:956–61.
- Song MH, Jin YF, Guo JS, et al. Application of whole-lesion intravoxel incoherent motion analysis using iZOOM DWI to differentiate malignant from benign thyroid nodules. *Acta Radiol*. 2019;60:1127–34.
- Wang Q, Guo Y, Zhang J, et al. Diagnostic value of high b-value (2000 s/mm²) DWI for thyroid micronodules. *Medicine (Baltimore)*. 2019;98:e14298.
- Castellana M, Castellana C, Treglia G, et al. Performance of five ultrasound risk stratification systems in selecting thyroid nodules for FNA. *J Clin Endocrinol Metab*. 2020;105:dgz170.
- Grani G, Lamartina L, Ascoli V, et al. Reducing the number of unnecessary thyroid biopsies while improving diagnostic accuracy: toward the "Right" TIRADS. *J Clin Endocrinol Metab*. 2019;104:95–102.
- Huh S, Lee HS, Yoon J, et al. Diagnostic performances and unnecessary US-FNA rates of various TIRADS after application of equal size thresholds. *Sci Rep*. 2020;10:10632.
- Peng JY, Pan FS, Wang W, et al. Malignancy risk stratification and FNA recommendations for thyroid nodules: a comparison of ACR TI-RADS, AACE/ACE/AME and ATA guidelines. *Am J Otolaryngol*. 2020;41:102625.
- Zhang WB, Xu HX, Zhang YF, et al. Comparisons of ACR TI-RADS, ATA guidelines, Kwak TI-RADS, and KTA/KSThR guidelines in malignancy risk stratification of thyroid nodules. *Clin Hemorheol Microcirc*. 2020;75:219–32.
- Huang Y, Hong Y, Xu W, Song K, Huang P. Contrast-enhanced ultrasound improves the accuracy of the ACR TI-RADS in the diagnosis of thyroid nodules located in the Isthmus. *Ultraschall Med*. 2022;43:599–607.
- Luo P, Fang Z, Zhang P, et al. Radiomics score combined with ACR TI-RADS in discriminating benign and malignant thyroid nodules based on ultrasound images: a retrospective study. *Diagnostics (Basel)*. 2021;11:1011.
- Padhani AR, Liu G, Koh DM, et al. Diffusion-weighted magnetic resonance imaging as a cancer biomarker: consensus and recommendations. *Neoplasia*. 2009;11:102–25.

32. Surov A, Meyer HJ, Wienke A. Correlation between apparent diffusion coefficient (ADC) and cellularity is different in several tumors: a meta-analysis. *Oncotarget*. 2017;8:59492–9.
33. Feeney C, Lingam RK, Lee V, Rahman F, Nagendran S. Non-EPI-DWI for detection, disease monitoring, and clinical decision-making in thyroid eye disease. *AJNR Am J Neuroradiol*. 2020;41:1466–72.
34. Meyer HJ, Wienke A, Surov A. Discrimination between malignant and benign thyroid tumors by diffusion-weighted imaging - a systematic review and meta analysis. *Magn Reson Imaging*. 2021;84:41–57.
35. Yuan L, Zhao P, Lin X, Yu T, Diao R, Ning G. T1 mapping and reduced field-of-view DWI at 3.0 T MRI for differentiation of thyroid papillary carcinoma from nodular goiter. *Clin Physiol Funct Imaging*. 2023;43:137–45.
36. Borowczyk M, Wolinski K, Wieckowska B, et al. Sonographic features differentiating follicular thyroid cancer from follicular Adenoma-A meta-analysis. *Cancers (Basel)*. 2021;13:938.
37. Smith J, Cheifetz RE, Schneiderei N, Berean K, Thomson T. Can cytology accurately predict benign follicular nodules? *Am J Surg*. 2005;189:592–5. discussion 595.

Publisher's Note

Springer Nature remains neutral with regard to jurisdictional claims in published maps and institutional affiliations.